AGU PUBLICATIONS

JGR

Journal of Geophysical Research: Oceans

RESEARCH ARTICLE

10.1002/2014JC010641

Key Points:
- A frontal event was observed in spring 2004, in the southeastern Beaufort Sea
- Sampling showed evidence of frontal intensification at both ends of the domain
- Vertical temperature structure will be shown to be largely dependent on fronts

Correspondence to:
C. Sévigny,
caroline.sevigny@ete.inrs.ca

Citation:
Sévigny, C., Y. Gratton, and P. S. Galbraith (2015), Frontal structures associated with coastal upwelling and ice-edge subduction events in southern Beaufort Sea during the Canadian Arctic Shelf Exchange Study, *J. Geophys. Res. Oceans*, *120*, 2523–2539, doi:10.1002/2014JC010641.

Received 10 DEC 2014
Accepted 6 MAR 2015
Accepted article online 13 MAR 2015
Published online 2 APR 2015

Frontal structures associated with coastal upwelling and ice-edge subduction events in southern Beaufort Sea during the Canadian Arctic Shelf Exchange Study

Caroline Sévigny[1], Yves Gratton[1], and Peter S. Galbraith[2]

[1]Institut National de la Recherche Scientifique—Centre Eau, Terre et Environnement, Québec, Québec, Canada, [2]Institut Maurice-Lamontagne, Mont-Joli, Québec, Canada

Abstract The near-surface temperature structure in the southeastern Beaufort Sea is shown to have been largely dependent on frontal dynamics in spring 2004, which may be typical for the region. Easterly wind events generated coastal upwelling along the Cap Bathurst peninsula; a recurring event in that area. Further west, a large mesoscale anticyclone simultaneously developed and subsequently controlled the sea-surface circulation in the central Amundsen Gulf. Sharp temperature and density fronts were created at the surface at both eastern and western ends of the domain. Sampling north of Cape Bathurst and Cape Parry showed evidence of frontal intensification. Frontal features were detected near the 50–200 m isobaths, at the mouth of the gulf, where density-compensated near-surface intrusions driven by agesotrophic vertical circulation were identified. These warm water tongues intruded into the outcropping isopycnal layers, which dipped down between 5 and 25 m over the Mackenzie Shelf. They then crossed the density surfaces with an inverse slope consistent with N/f as predicted for quasi-geostrophic flows. The front event ended prior to the breakup of the landfast-ice bridge in late June with sea-surface temperature undergoing quick and widespread changes throughout the Amundsen Gulf.

1. Introduction

Some regions of the Arctic Ocean are particularly susceptible to coastal upwelling events that bring to the surface saline, nutrient-rich waters, and considerably changes the sea-surface distribution of oceanographic properties. One such region is located east of Cape Bathurst, a peninsula in the southeastern Beaufort Sea (Figure 1a). This area provides favorable conditions for topographically enhanced shelf break upwelling under prevailing easterly winds [*Williams and Carmack*, 2008; *Ingram et al*., 2008]. Although episodic, these events can determine regional dynamics on larger scales. As an upwelled water mass undergoes geostrophic adjustment, an alongshelf jet is generated. The process creates a sharp, near-surface horizontal density gradient with slanted isopycnals in the near-coast area. When the resulting large-scale straining field associated with the front is sufficiently strong to promote surface frontogenesis (i.e., rapid intensification of frontal gradients), both upwelling and downwelling occur and transfer water properties and tracers between the surface mixed layer and the ocean interior [*Hoskins and Bretherton*, 1972; *Spall*, 1995; *Pollard and Regier*, 1992]. This enhanced vertical exchange can have a significant impact on biological productivity [e.g., *Zakardjian and Prieur*, 1998; *Nagai et al*., 2008; *Johnston et al*., 2009], especially in high-latitude northern seas where nutrients are the main limiting factor of the phytoplankton growth [*Tremblay and Gagnon*, 2009]. Upper-ocean submesoscale processes ($\sim$1 km) related to sharp density fronts are regarded as the key mechanism of the forward energy cascade from mesoscale motions (10–100 km) to dissipation at microscales ($<$1 m) [i.e., *Mahadevan and Tandon*, 2006; *McWilliams et al*., 2009; *Capet et al*., 2008a; *Molemaker et al*., 2010]. There is increasing observational evidence that three-dimensional vertical mixing is intensified near fronts [e.g., *D'Asaro et al*., 2011; *Nagai et al*., 2012; *Johnston et al*., 2011; *Thomas et al*., 2013], which can further enhance biological activity and nutrients supply [e.g., *Nagai et al*., 2008]. The objective of this paper is to understand how the Amundsen Gulf region is affected by the frontal structure that was observed near Cape Bathurst during the Canadian Arctic Shelf Exchange Study (CASES).

1.1. Southeastern Beaufort Sea and Amundsen Gulf in Spring 2004

In spring 2004 (Canadian Arctic Shelf Exchange Study 2003–2004), [*Barber et al*., 2008] and fall 2007 (IPY—Circumpolar Flaw Lead System Study 2007–2008) [*Barber et al*., 2010], oceanographic surveys were carried

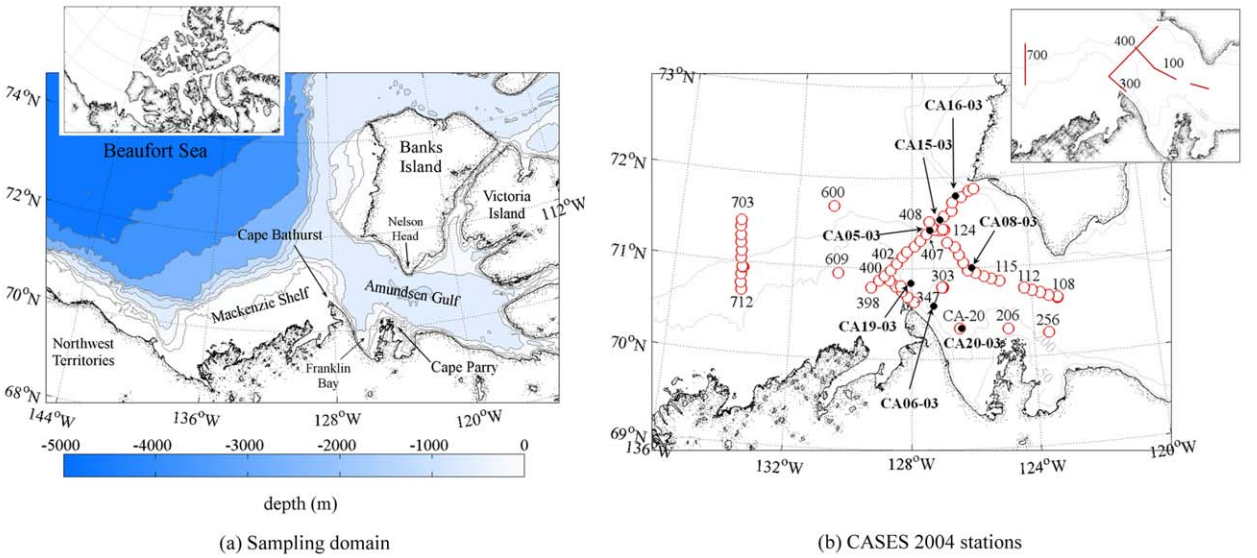

Figure 1. (a) Bathymetry of southeastern Beaufort Sea and (b) position of moorings (black dots) and oceanographic stations (red circles) sampled in June 2004. The insert in Figure 1b shows the main CTD transects.

out in the southeastern Beaufort Sea and Amundsen Gulf, on and near to the Mackenzie Shelf. Both were conducted under upwelling-favorable winds, which were more intense and persistent in 2007. During this 2007 International Polar Year (IPY), sampling revealed the legacy of a major upwelling event near the continental coasts (i.e., high salinity of surface waters), which was triggered by unusual atmospheric conditions that also impacted on the Arctic multiyear sea ice cover [*Tremblay et al*., 2011; *Perovich et al*., 2008; *Stroeve et al*., 2008]. Unfortunately, the survey reached Amundsen Gulf weeks after the initial uplift of the thermocline, once upwelled dense waters had largely spread over the entire shelf north of Cape Bathurst (out to the 200 m bathymetry line) [*Tremblay et al*., 2011]. No conclusion can thus be drawn about the processes that controlled the formation and evolution of this event. However, as it will be shown below, the 2004 open-water survey was conducted during the course of a moderate, but nevertheless important, coastal upwelling that considerably modified the ocean dynamics and determined the late spring-early summer physical conditions in the southeastern Beaufort Sea.

Here we describe the context underlying the coastal upwelling observed in spring 2004 within the Amundsen Gulf, the near-surface circulation that followed the generation and evolution of surface density fronts, and the resulting subsurface dynamics. Special emphasis is given to the vertical temperature structure of the upper ocean (0–100 m), which will be shown to be largely dependent on front formation. The upper layer in the southern Canada basin consists of a Polar-Mixed layer (salinity <31, 0–50 m) and an upper halocline, within which is found a local temperature maximum composed of Pacific origin water ($31 < S < 32$, 50–100 m) [*Carmack and Kulikov*, 1998; *McLaughlin et al*., 1996, 2004]. Early summer-late fall water mass structure is also typified by a near-surface temperature maximum that is believed to take shape during the melting period, with solar radiation warming waters beneath the newly formed seasonal halocline [*Jackson et al*., 2010]. Similar temperature anomalies observed in the Amundsen Gulf will be shown here, but their formation will be argued to be linked to the complex circulation that develops at the shelf break while the front evolves. This paper aims to provide a brief description of some typical frontal processes active in southeastern Beaufort Sea under upwelling-favorable wind conditions. It is important to note that the sampling program was not designed to study fronts but was rather planned for the more general, larger scales, biogeochemical-ice objectives of the Canadian Arctic Shelf Exchange Study. We were fortunate enough to sample during a frontogenesis situation and fortunate enough to have access to a few high resolution (<1 km) Moving Vehicle Profiler CTD sections. Even if limited inferences and conclusions can be drawn from this partial data set, we will supplement it with satellite images and mooring data to present a clear sketch of the frontal structures found in Amundsen Gulf during June 2004.

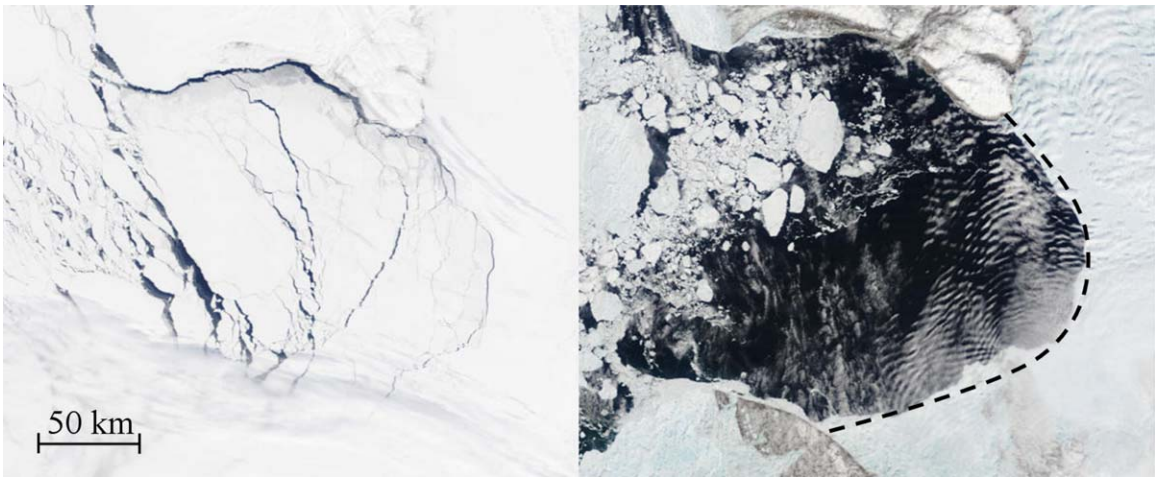

Figure 2. Terra/MODIS image of the Amundsen Gulf on (left) 20 May and (right) 9 June 2004. Black dotted line indicates the location of the landfast-ice bridge.

2. Measurements and Methods

2.1. Survey Overview

As part of the CASES sampling program, a broad survey of the southeastern Beaufort Sea and Mackenzie Shelf was carried out from the *CCGS Amundsen* in spring 2004. The ship left its overwintering site located in the central Franklin Bay on 1 June, a few days after the opening of the Cape Bathurst polynya (Figure 2). Sampling begun at the eastern edge of the Amundsen Gulf, along the (recurrent) landfast ice bridge that extended from Banks Island to the continent [*CIS*, 2007], and proceeded further west, reaching the northern flank of Cape Bathurst. The sea ice concentration in the sampling domain rapidly declined to 25% by mid-June and ∼3% by mid-July [*Forest et al*., 2008]. According to Earth Observing System (EOS) Moderate Resolution Imaging Spectroradiometer (MODIS) data, a few shear lines appeared at the ice edge on the 25 and 28 June, just prior to the breakup of the ice bridge, leading to the export of sea ice out of the eastern part of the Amundsen Gulf (http://earthdata.nasa.gov/data/near-real-time-data/rapid-response). Here only data recorded during the opening phase of the polynya in June 2004 are discussed.

2.2. Hydrography: CTD and Moorings

Between 1 and 20 June 2004, 42 open-water stations along four main transects were sampled in the Amundsen Gulf and the south-eastern Beaufort Sea (Figure 1b). At each site, a vertical profile of temperature, salinity, and dissolved oxygen was obtained using a CTD-rosette system (*SeaBird* SBE-911, 24 Hz resolution, nominal fall speed of 1.0 m s^{-1}) equipped with an oxygen sensor (*SeaBird* SBE-43) deployed alongside the ship. Two high resolution transects were also sampled with help of a Moving Vessel Profiler (MVP-300/1700, *Brooke Ocean Technology Limited*) north of Cape Bathurst, along and across the southern section of the mouth of Amundsen Gulf (line M100, between stations 402 and 407, and line M300, between stations 400 and 303; Figure 1b). The MVP is a towed vehicle that free falls vertically (∼5 m s^{-1}). When the ship steams at 5–6 knots in shallow water (<300 m), a cast takes only 2–3 min, yielding a cast every ∼0.5–0.7 km (compare with 10 km typical spacing between CTD-rosette stations). The MVP was equipped with a CTD *SeaBird*−9*Plus* coupled to an oxygen sensor and a fluorometer. After an initial quality control test based on UNESCO's algorithm standards [*Intergovernmental Oceanographic Commission*, 2010], the data were low-pass filtered at 1 Hz using a phase-preserving fourth-order Butterworth filter. Potential temperature, θ, and potential density, σ_θ (referenced to sea surface), were then computed.

Several moorings carrying oceanographic sensors where deployed at key locations in the southeastern Beaufort Sea prior to the overwintering period (black dots, Figure 1b). They provided a continuous record of temperature and salinity (Alec CT) at a time step of 10 min from October 2003 to mid-July 2004. Except at instruments line CA03, upward looking Acoustic Doppler Current Profiler (*RD Instrument Workhorse Sentinel* 300 kHz) were also deployed at ∼100 m depth, providing currents to the near-surface with a vertical bin size of 8 m and a temporal resolution of ∼30 min. Near-surface bins were rejected to avoid contamination induced by ice motion.

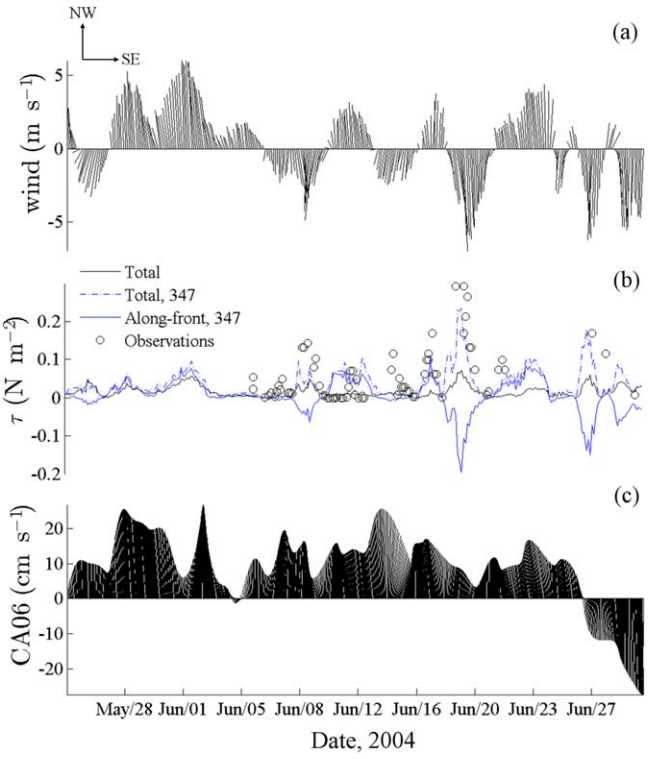

Figure 3. (a) Mean wind velocity and (b) wind stress calculated from the 3 hourly average NCEP reanalysis data over the Amundsen Gulf (black) and at station 347 (blue). Wind stress computed from ship based observations is added for comparison (black dots). (c) Averaged along-front current recorded at mooring CA06 in the 0–30 m depth layer. Velocities are rotated into the frontal coordinate frame according to the northwest-southeast orientation of the Cape Bathurst upwelling area observed on 13 June.

2.3. Sea-Surface Temperature

Maps of daily sea-surface temperature (SST) were generated using of the National Oceanic and Atmospheric Administration (NOAA) Advanced Very High Resolution Radiometer (AVHRR) satellite images available from the Department of Fisheries and Oceans (DFO) Maurice Lamontagne Institute remote sensing laboratory. The procedure, described by *Galbraith and Larouche* [2011], creates georeferenced images that are projected onto a grid of 1 km spatial resolution. A combination of tests based on the pixel albedo and temperatures is used to ensure cloud-free, sea ice-free data.

2.4. Meteorological Data

Meteorological data were obtained from the 3 hourly average NCEP–NARR database (http://www.esrl.noaa.gov/psd/data/gridded/data.narr.html). Wind speed and direction agreed well with the data acquired by the ship-mounted weather station of the *CCGS Amundsen* (Figure 3).

3. Results

3.1. Upwelling and Fronts in the Amundsen Gulf: Spring 2004

In the late May and early June 2004, two easterly wind events (nominal speed 4.9–6.4 m s^{-1}) quickly opened a large ice-free area in south-western Amundsen Gulf (Figure 2) and favored the development of a coastal upwelling north of Cape Bathurst, similar to those observed at the same location in the past [*Williams and Carmack*, 2008].

3.1.1 Coastal Upwelling

Between 25 May and 6 June, the 0–30 m average currents off Cape Bathurst revealed a strong north-westward transport along the coast (mean speed/direction 12.5 cm s^{-1}/293°N and 13.9 cm s^{-1}/286°N at CA06 and CA20, respectively; cf. Figure 1b for stations position), where upwelled waters generally reach the surface [*Williams and Carmack*, 2008]. Further north (CA05, CA08, CA15, CA16; cf. Figure 1b for stations position), the currents remained negligible (<2 cm s^{-1}) and are representative of the breakup period (15 April to 15 July) [*Barber et al*., 2008]. At the same time, the potential density recorded at 30 m increased abruptly off the tip of the peninsula (CA19; cf. Figure 1b for location), ranging from σ_θ = 24.6 to 25.9 kg m^{-3} (event E1, Figure 4). A similar, although smaller increase is also observed at the shelf break (CA03, 28 m) few days later (event E2, Figure 4). No significant changes are detected beyond the 200 m isobath (CA15). These observations provide evidence of the upwelling whose influence seems to be confined to the Mackenzie Shelf, between the 50 and the 200 m isobaths.

The survey began on the eastern side of the Amundsen Gulf and moved westward along transect 100, reaching the mouth of the Gulf by mid-June. Hence, the Cape Bathurst area was only sampled at the end of June, once survey progressed toward the mainland (following transect 400). The SST recorded on 13 June (the first image free of cloud and sea ice of the survey) shows a noticeable upwelling zone along the Mackenzie shelf, with a thin swath of cold (T < 0°C) upwelled waters extending ~30 km inside the Gulf (2008;

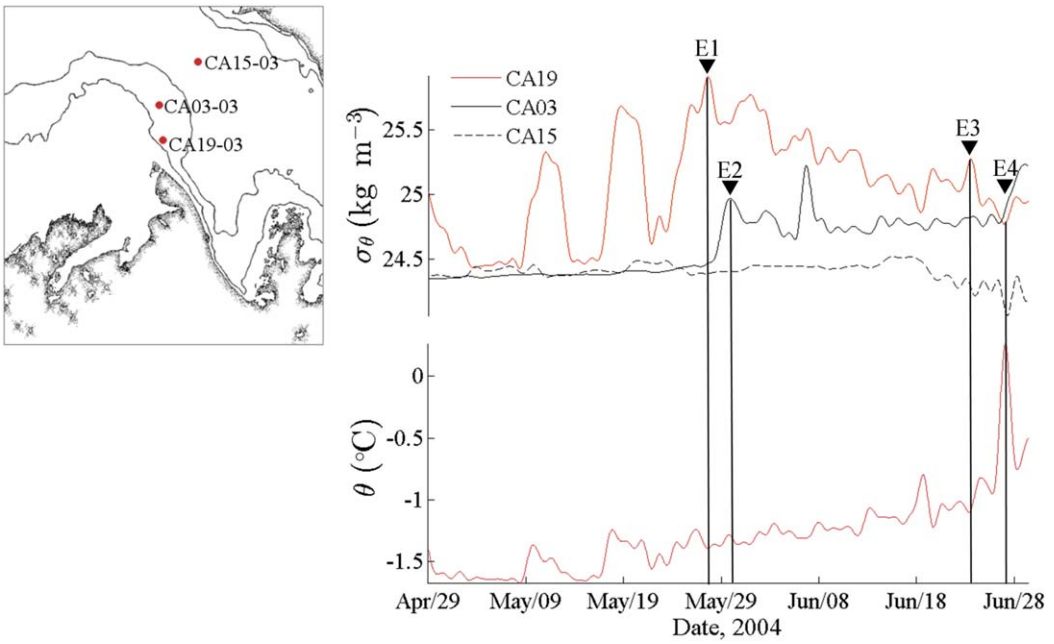

Figure 4. (top) Potential density time series at CA19 (30 m), CA03 (28 m), andCA15 (20 m) and (bottom) potential temperature at CA19(30 m) . Arrow heads and vertical lines indicate main events discussed in the text.

black double-headed arrow, Figure 5). This corresponds to the area shown by *Williams and Carmack* [2008] where enhanced upwelling is forced by the adjustment of the along-shelf flow, part of the upwelling circulation, to the isobath divergence at the cape. The horizontal distribution of σ_θ at 5 m obtained from ship-based observations revealed water density of 25.2 kg m^{-3} along this strip (transect 300, Figure 6a), which decreased to 24.5 kg m^{-3} at the center of the mouth and remained constant thereafter. At 30 m, the high density waters are still noticeable around the peninsula (Figure 6b). The event of the late of May-early June has thus influenced the upper-ocean structure of the southwestern Amundsen Gulf for 3–4 weeks, at least until the survey reached the Mackenzie Shelf on 21–22 June (transect 300).

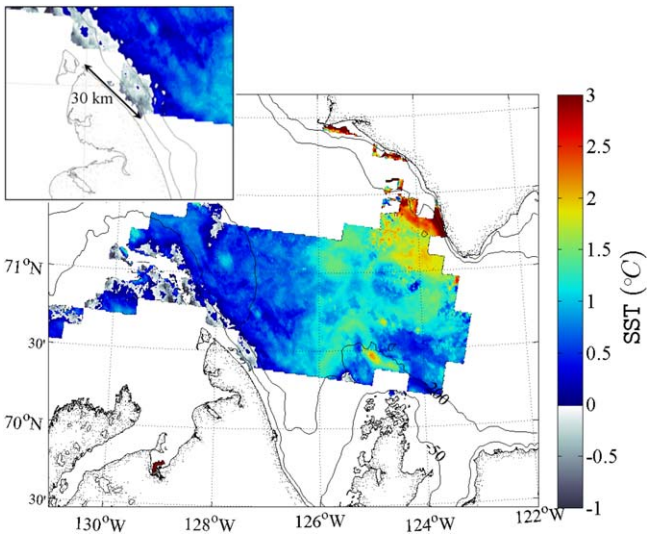

Figure 5. Sea-surface temperature (SST) from the Advanced Very High Resolution Radiometer for 13 June 2004. A ~30 km long thin strip of cold upwelled waters is observed offshore of the northeastern coast of Cape Bathurst (black double-headed arrow).

3.1.2. Frontal Dynamics: Upper-Ocean Structure and Evolution

The SST maps and mooring data provide insight about the development and evolution of the surface ocean structures induced by the upwelled high density waters. Figure 7 shows representative daily SST maps for the second and third weeks of June 2004. Vectors give the corresponding weekly averaged currents recorded by ADCP in the 0–30 m depth layer.

3.1.2.1. SST Distribution: 10–24 June 2004

Seasonal warming of the ocean surface begins at the shelf margins of the Cape Bathurst polynya (Figure 7). This warming is limited to the eastern part of the gulf and does not significantly impact the upwelling area located south of the 50 m isobath (label CB-1, Figure 7). The >2°C surface waters observed at the landfast

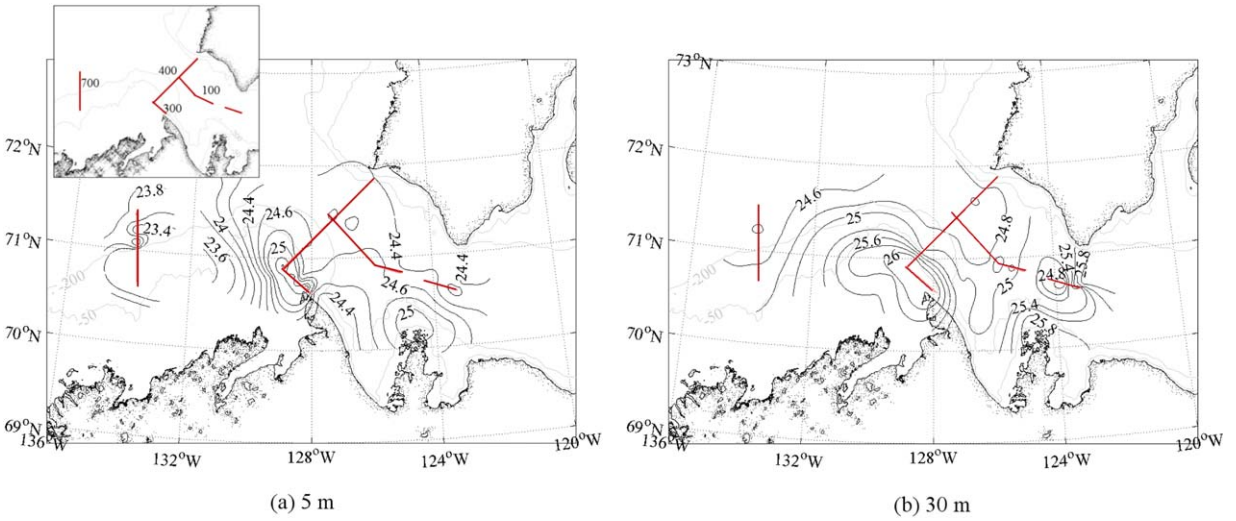

Figure 6. Horizontal distribution of potential density at (a) 5 and (b) 30 m obtained by (ordinary) kriging of CTD data. Only interpolation having an estimated error (or variance) $\leq$0.15 kg^2 m^{-6} are shown.

ice-edge of Franklin Bay seem rather transported offshore by the upwelling circulation. Those waters are presumably advected northwestward from the eastern flank of the cape (mooring CA06), along the 200 m isobath that encloses the high density area (label CB-2, Figure 7b). The northern half of the mouth remained covered with large ice floes during the first 3 weeks of June.

Concurrent with the upwelling, a large anticyclone developed southwest of Nelson Head and quickly spread the surface warm waters close to Banks Island and Franklin Bay (label AE, Figure 7). This mesoscale eddy (≈40 km diameter) was only partly sampled by CTD stations, limited to its southern third. The σ_θ distribution at 30 m nonetheless shows a low density area near the cold water core noticeable in the middle of the Gulf on the SST map of June 15 (and labeled AE; Figures 6b and 7a). Currents recorded at stations CA15 and CA16 (0–30 m) are well correlated with the large-scale near-surface flow fields associated with this eddying pattern (Figure 7a).

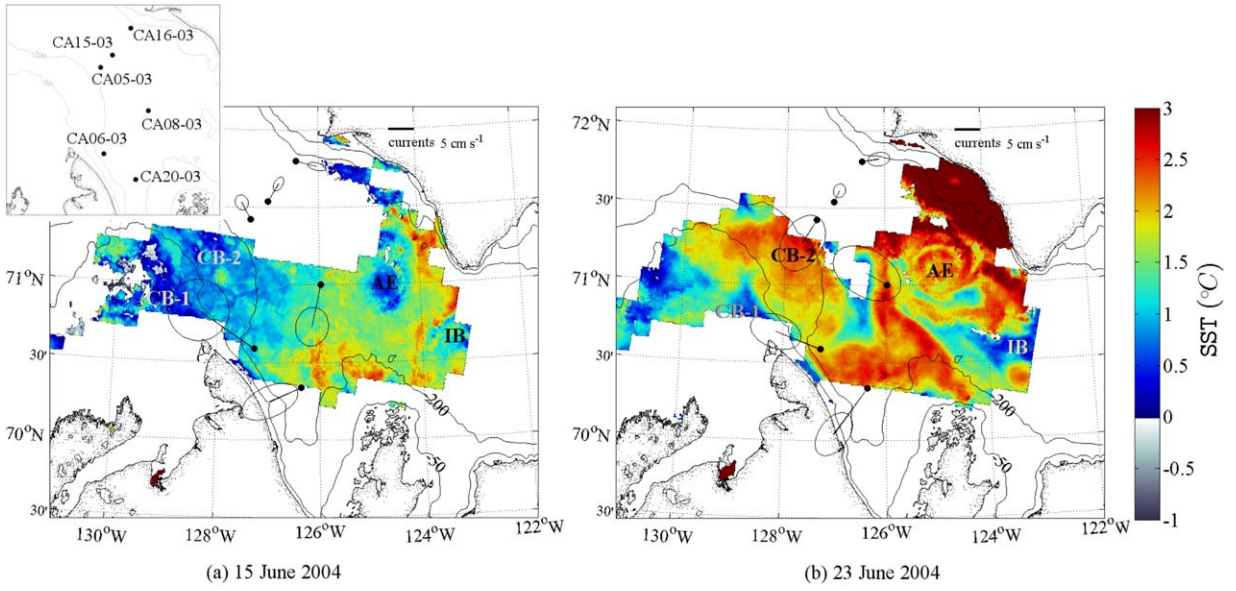

Figure 7. Sea-surface temperature (SST) from the Advanced Very High Resolution Radiometer for (a) 15 June (second week of survey) and (b) 23 June 2004 (third week of survey). Black dots are moorings station, vectors the weekly averaged current (0–30 m), and ellipsis the currents standard deviation. CB-1: upwelling area. CB-2: the extended zone along the 200 m isobath, north of Cape Bathurst. AE: the mesoscale anticyclonic eddy. IB: the marginal area of near-freezing waters north of Cape Parry, at the ice bridge edge.

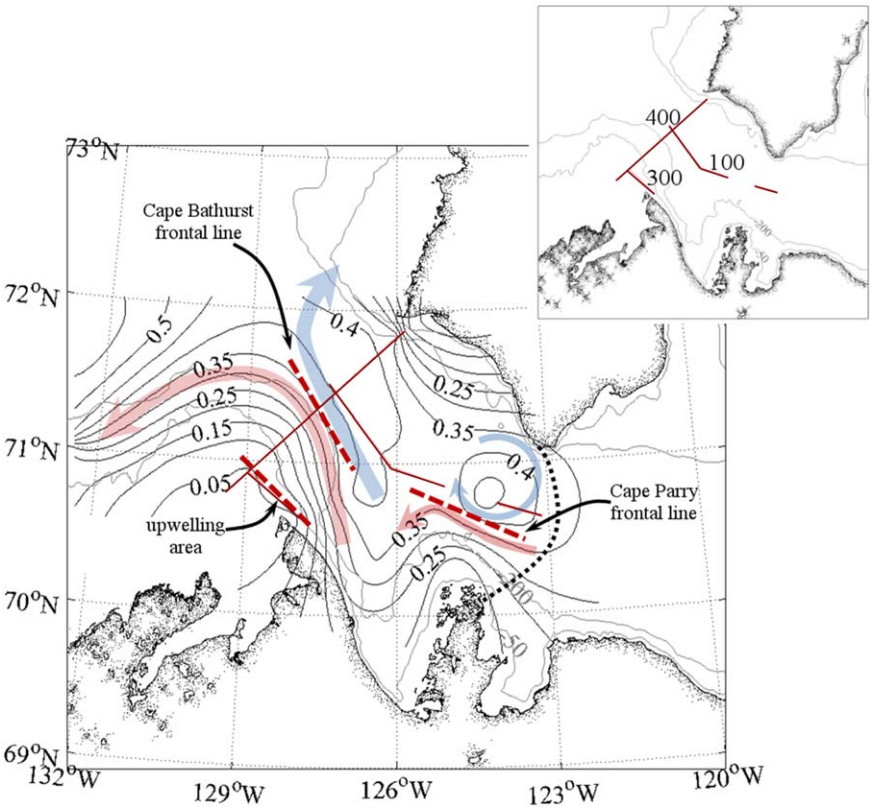

Figure 8. Horizontal distribution of dynamic height at 5 m (ordinary kriging) and schematic representation of the near-surface dynamics in Amundsen Gulf in spring 2004. Only interpolations having an estimated error (or variance) of $\leq$0.015 m^2 are shown. Arrows indicate cyclonic (red) and anticylconic (blue) circulation. The black-dotted line indicates the geographic location of the ice bridge and solid red lines in the top insert show the main CTD transects. Frontal lines are shown by the red dashed lines, as the offshore limit of the upwelling area that follows the 50 m isobath.

By mid-June, a marginal area of near-freezing temperature was forming at the ice bridge edge as $>2^{\circ}$C near-coastal surface waters were transported southeastward by the gyre-like circulation. This area extended south as far as the outer continental shelf where a strong horizontal gradient in sea-surface temperature was observed (label IB, Figure 7b). The latter coincided with the abrupt change in σ_θ observed north of Cape Parry (Figure 6).

3.1.2.2. Circulation and Dynamic Height

The SST maps show numerous singularities that suggest the development of surface fronts in the wake of the coastal upwelling of June 2004: the upwelling zone, which extended to the 200 m isobath (label CB-1 and CB-2); the mesoscale anticyclonic eddy (label AE); and the marginal area of near-freezing temperature north of Cape Parry, at the ice bridge edge (label IB, Figure 7). These areas explain the high density gradients observed in the horizontal distribution of σ_θ at 5 and 30 m (Figure 6). The near-surface circulation in Amundsen Gulf can thus be deduced from CTD data and, consequently, geostrophic flow can be, to a first approximation, considered representative of the frontal event (i.e., using the quasi-geostrophic approximation).

A map of dynamic height at 5 m depth (referenced to near bottom) is used to provide a qualitative description of the surface circulation, the moorings being spaced too sparsely to permit a complete regional flow pattern characterization. The geostrophic current $\mathbf{u}_g=(u_g, v_g, 0)$ relative to the reference level is calculated from the gradient of the dynamic height along pressure surfaces,

$$f\mathbf{k}\times\mathbf{u}_g=-\nabla_h D. \tag{1}$$

with f, the Coriolis parameter, $\nabla_h=(\partial/\partial x, \partial/\partial y, 0)$ and $dD=g\,dz=1/\rho\,dp$, the dynamic height computed from the CTD recorded density ρ, where g denotes the gravitational acceleration and p, the pressure.

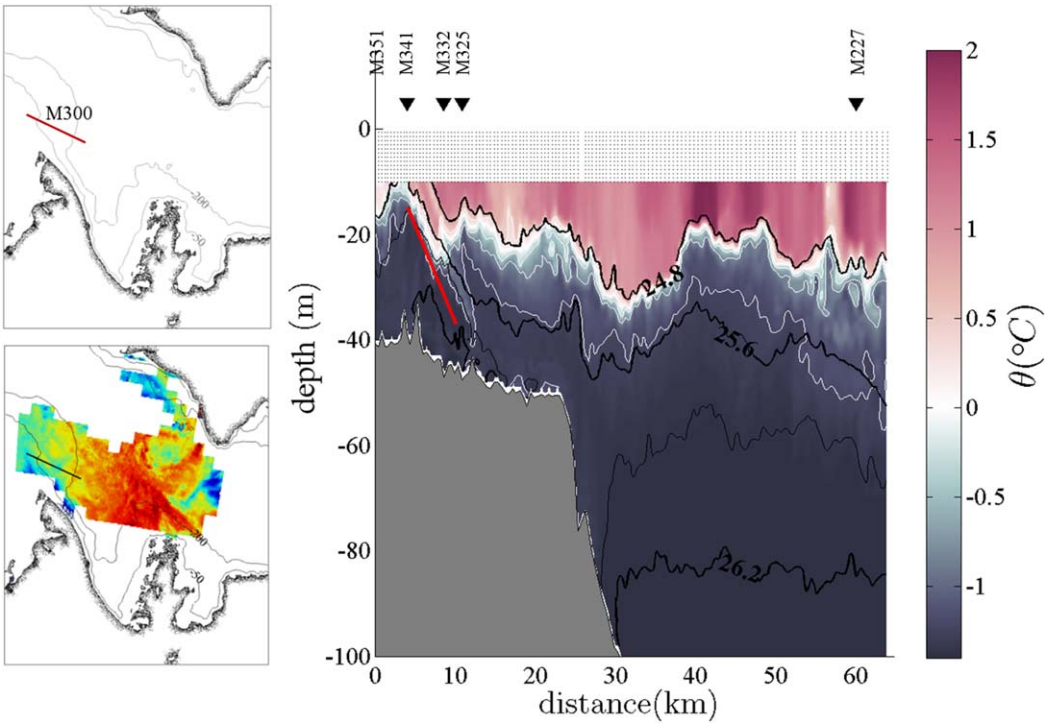

Figure 9. Vertical distribution of potential temperature obtained by cubic interpolation along MVP line M300 (from west to east, sampled on 20–21 June 2004). Black lines indicate isopycnals of 24.8, 25.6, 26.0, and 26.2 kg m^{-3}; dotted lines show MVP stations along the transect; triangles show the position of the stations mentioned in the text; and the red line indicates a slope of $f/N = 3.7 \times 10^{-3}$ (with $N = N(15\ m)$ at the center of the intrusive feature). SST of 17 June is annexed on the bottom left side of the figure.

Results are presented in Figure 8. Offshore of Cape Bathurst, a cyclonic circulation centered on transect 300 developed. Together with a clockwise flow in the middle of the mouth, they created a confluence zone at the Mackenzie shelf break hereafter named Cape Bathurst frontal line. The 200 m isobath marks the northward limit of the density front generated by the upwelled waters. Further east, the large anticyclonic eddy observed in satellite data is well defined by the low dynamic height region visible south of Nelson Head, although somewhat geographically misplaced due to sparse sampling. A second confluence zone appeared at its southern flank, delimiting also by cyclonic circulation to its south. It corresponds to the Cape Parry frontal line identified in the Figure 8. A careful analysis of CTD data will provide insight into the subsurface dynamics induced in the vicinity of these fronts.

3.1.3. Subsurface Dynamics

MVP lines were sampled during the second week of June (Figures 9 and 10). Line M300 crosses the Mackenzie shelf at the tip of the peninsula, north of the upwelling area observed in the SST images (CB-1, Figure 7). Between stations M325 and M341, the 25.6 kg m^{-3} isopycnal outcrops into the mixed layer and falls abruptly following a slope of 2.8×10^{-3} on the continental shelf (Figure 9). A warm water tongue 4.6 km long and 25 m thick can be seen next to this constant density layer (just above the red line traced in the right plot of Figure 9), taking the form of a density-compensated near-surface intrusion that crosses σ_θ surfaces from 25.3 kg m^{-3} at station M332 ($\theta \sim 1.1^{\circ}$C) to 25.9 kg m^{-3} at M325 ($\theta \sim -0.9^{\circ}$C). Double-diffusion, which is commonly invoked to explain interisopycnal displacements [e.g., *May and Kelley*, 2001], is not responsible for this intrusive feature as salinity increases with depth along the filament path. Instead, active frontal dynamics are conceivably at work.

In quasi-geostrophic theory, an ageostrophic vertical circulation that develops in the confluent flow acts to restore the thermal wind balance by actively tilting isopycnals toward the horizontal (i.e., restratification) and accelerating the geostrophic current, therefore counteracting the strengthening of surface horizontal density gradient [*Capet et al.*, 2008a]. In so doing, this frontogenetic circulation, with downwelling on the dense (cyclonic) side of the front and upwelling on the light (anticyclonic) side of the front, locally organizes the vertical and horizontal velocity fields to preserve along-isopycnal flow [*Klein et al.*, 1998]. Passive scalars,

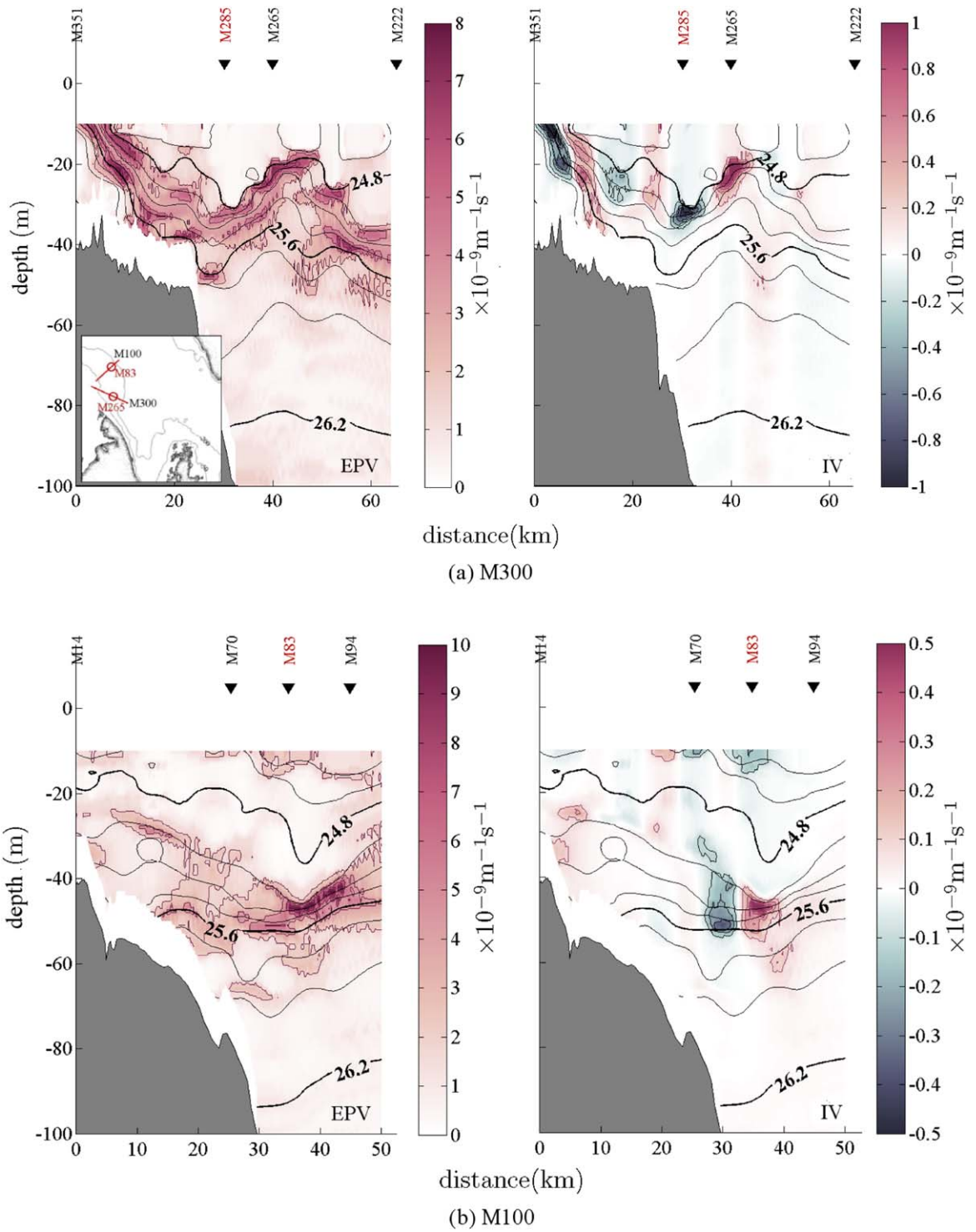

Figure 10. (left) Ertel potential vorticity and (right) isentropic vorticity along MVP line (a) M300 and (b) M100, both sampled 17–21 June 2004. Black lines indicate isopycnals step of 0.1 kg m^{-3} below 24.8 kg m^{-3} and of 0.2 kg m^{-3} above. Insert localizes stations M83 (line M100) and M265 (line M300; red circles).

denoted here by ϕ, are thus substantially stirred following a fluid particle trajectory. Elongated filaments then result from the combined effects of the large-scale deformation field (the confluence) and the geostrophic vertical shear [*Smith and Ferrari*, 2009]. Their horizontal-to-vertical scale ratio, α, is proportional to the ratio of shear over strain, which is centered around a mean value of *N/f* [*Smith and Ferrari*, 2009; *Haynes and*

Anglade, 1997]. In turbulent geostrophic flow, a three-dimensional cascade of tracer variance $\overline{\phi'^2}$ is observed, the thickness of the anomalies being determined by the scale of the vertical (diffusing) mixing. Intrusion slopes observed over the Mackenzie Shelf closely follow the aspect ratio estimated for the local temperature maximum depth (f/N(15 m) $=3.7\times10^{-3}$; the red line in Figure 9), which is indicative of the subsurface processes active near the Cape Bathurst frontal line. Warm waters advected from the southern edge of the Cape Bathurst polynya by the (cyclonic) coastal upwelling circulation are hence pulled down below the mixed layer by the ageostrophic fields active at shelf break. The core of this $\theta > 0^{\circ}$ C water mass travels along the outcropping isopycnal layers 24.8–25.4 kg m^{-3} as they dip down from 5 to 25 m, leaving numerous intrusive features near the 200 m isobath, northeast of the peninsula (not shown).

3.1.3.1. Ertel Potential Vorticity

Subsurface circulation in the southern part of the mouth of Amundsen Gulf can further be deduced using Ertel potential vorticity (PV), since it is conserved following a water particle in nondissipative and adiabatic motion. It is defined as

$$Q=\frac{\xi+2\Omega}{\rho_0}\cdot\nabla\sigma_\theta \tag{2}$$

with ρ_0, the reference density (calculated as the mean value of the transect), $\xi=\nabla\times\mathbf{u}$, and $\mathbf{u}=(u,v,w)$, $2\Omega=(0,f_h,f)$ in (x, y, z) coordinates with z vertically upward. In a f-plane, using the hydrostatic approximation and geostrophy, and approximating $\mathbf{u}$ by the geostrophic velocity $\mathbf{u}_g$, it is possible to write

$$-\frac{f}{g}\frac{\partial\mathbf{u}_g}{\partial z}=\frac{1}{\rho_0}\nabla_h\sigma_\theta, \tag{3}$$

and the preceding expression reduces to

$$Q=\frac{N^2}{g}\left(f+\xi_g-fF_g\right), \tag{4}$$

where ξ_g is the geostrophic relative vorticity, $N=(-g/\rho_0)\partial\rho/\partial z$, the Brunt-Väisälä frequency, and F_g, the geostrophic Froude number, which accounts for the conversion of horizontal vorticity to vertical vorticity through vertical shear (vortex twisting or tilting term),

$$F_g=\frac{1}{N^2}\left[\left(\frac{\partial u_g}{\partial z}\right)^2+\left(\frac{\partial v_g}{\partial z}\right)^2\right]. \tag{5}$$

The geostrophic Froude number becomes important when isopycnals slope strongly across the current and is implicitly accounted for in relative vorticity calculated isopycnally (isentropic vorticity, IV) [*Pollard and Regier*, 1992],

$$IV=\xi_g-fF_g=\left(\frac{\partial v_g}{\partial x}-\frac{\partial u_g}{\partial y}\right)\Big|_{\sigma_\theta=\text{const.}}, \tag{6}$$

as it represents a coordinate adjustment when working in a vertical pressure coordinate.

By invoking geostrophy, the characteristic scales of the mean velocity field are assumed to be large compare to the Rossby radius of deformation as expected for meso and large-scale flows. While it is suitable for the initial phase of the front formation, this assumption no longer applies once front is further sharpened and submesoscale features develop. In such conditions, the restoring effect of the ageostrophic components of the velocity fields, u_a and v_a, start to play a dynamic role by changing the stratification and the geostrophic velocity field. This is particularly true near the surface where are concentrated the ageostrophic processes, the dynamics in the ocean interior remaining rather close to geostrophy [*Klein et al.*, 2008]. The following description is therefore restricted to the initial development and evolution of the frontal dynamics observed in the southeastern Beaufort Sea. It only gives a simplified description of the processes active in the domain and fails to diagnose the leading order features that may appear in the surface layer.

Ertel potential vorticity computed along MVP transects M100 and M300 shows subsurface maxima near the 100–150 m isobaths north of Cape Bathurst, where the 24.8–25.2 kg m^{-3} layer thins and σ_θ rises to the surface. These maxima are tied to cyclonic anomalies and positive inshore-offshore potential vorticity gradient,

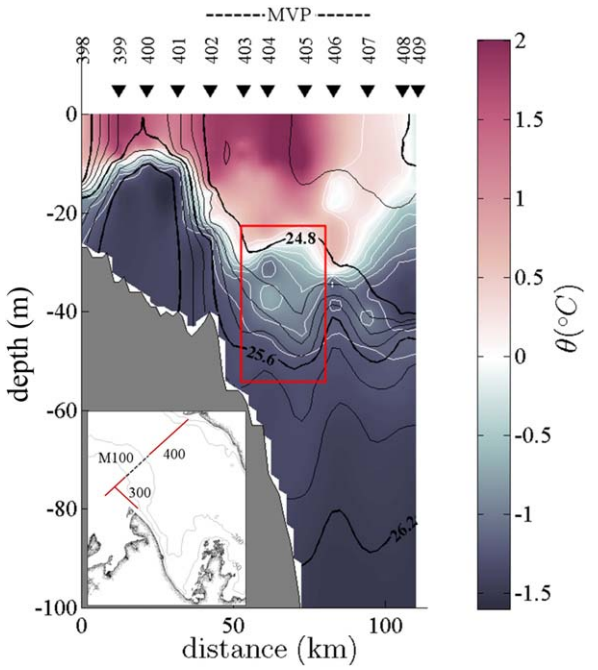

Figure 11. Vertical distribution of potential temperature obtained by cubic interpolation along line 400 (from south to north, sampled on 12–17 June 2004). Black lines indicate isopycnals of 24.6–26.2 kg m^{-3} steps of 0.1 kg m^{-3} prior to 24.8 kg m^{-3} and 0.2 kg m^{-3} thereafter; triangles, the position of each named station; and the horizontal dotted line, the approximative location of MVP transect M100. The red box indicates the isopycnal rising discussed in the text.

the PV increasing from 2.2 to 7.2×10^{-9} m^{-1} s^{-1} between stations M285 and M265 (line M300, Figure 10a) and from 2.4 to 9.0 ×10^{-9} m^{-1} s^{-1} between stations M70 and M83 further west (line M100, Figure 10b). As they reach values close to those observed at the frontal outcrop (∼8.3×10^{-9} m^{-1} s^{-1}, line M300), the highly stratified waters detected at depth, in the middle of transects, most probably originate from the Cape Bathurst peninsula area. This suggests that thermocline waters were advected away from the coast by the meandering circulation that developed on the shelf because of the instability of the along-front current.

The CTD section 400 crossed the mouth of Amundsen Gulf northwestward of the SST <0°C zone and overlapped MVP transect M100 between stations 402 and 407 where some isopycnals rose to the surface (Figure 11). Along this transect, the stretched 24.8–25.6 kg m^{-3} layer outcrops near the 30–40 m isobaths at station 400, the westernmost station of transect 300 centered on the front. Waters sampled at $\sigma_\theta > 25.6$ kg m^{-3} over the Mackenzie shelf appear to have been advected cross shelf by the wind-driven upwelling circulation, as denser waters of ∼26.4 kg m^{-3} are characteristic of those usually found below 100–110 m in the central Amundsen Gulf. The weakly stratified waters observed at 20–40 m depth near the shelf break (i.e., at stations 403–406, Figure 11) show physical properties similar to those found flowing northwestward from stations CA20 and 303, along the Cape Bathurst frontal line. It seems that the large-scale eddying circulation along the continental margin (50–200 m isobaths) carried warm surface waters westward, offshore of this patch of $\theta < 0^\circ$C (red box, Figure 11). The near-surface $\theta > 0^\circ$C intrusive features identified along the 200 m isobath may have resulted from the slant-wise ageostrophic circulation that develops within a meander. They are recognizable by the local positive anomaly of potential vorticity detected below the mixed layer in the vicinity of the midtransect station in Figure 10b (station M83).

3.1.3.2. Near-Surface Temperature Maximum?

Frontal subduction can explain another feature observed in the region in 2004. Near-surface temperature maximum commonly observed in the Canada basin is thought to be linked to solar radiation trapped below the summer halocline once sea ice meltwater spread on the surface ocean. Called NSTM by *Jackson et al.* [2010], this peculiar feature has a salinity less than 31, which distinguishes it from Pacific origin water, and a maximum temperature that is at least 0.2°C above the freezing temperature and 0.1°C above the minimum temperature of the underlying layer. They first appeared between mid-June and mid-July and remained at relatively shallow depths until the end of August, when they were found at depths greater than 20 m. By September, the intrusions had gradually cooled and deepened under Ekman pumping, winter storms, and advection. The summer halocline located 3–4 m above the NSTM prevented a fast erosion of the heat stored at the maximum temperature depth until penetrative convection (from brine rejection), air-ocean and ice-ocean stresses succeed to deepen the surface mixed layer. Persistent, year-round intrusions can nonetheless be observed in the central Canada Basin (north of 75°N) where Ekman pumping within the convergent Beaufort Gyre causes a downwelling rate of ∼3.5 m $month^{-1}$ [*McPhee et al.*, 2009].

In spring 2004 (6–30 June), some surface intrusions were detected along the Mackenzie Shelf break at an averaged depth of 24.7 (23.8; 25.0) m (with their 2.5 and 97.5‰), which is deeper than the depth reported

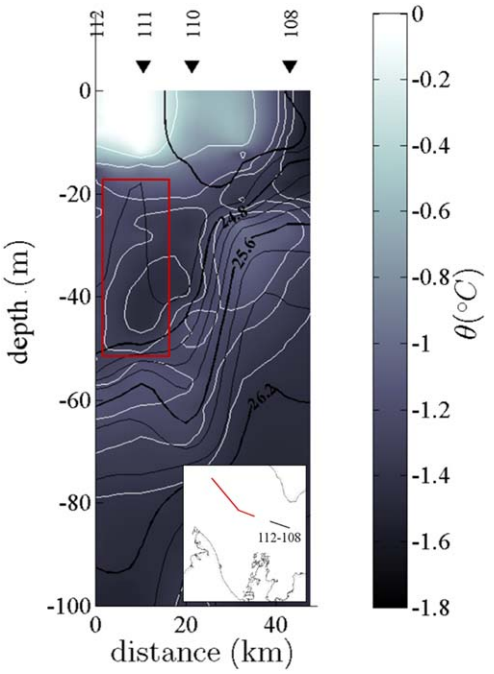

Figure 12. Vertical distribution of potential temperature obtained by ordinary kriging along the eastern section of line 100 (from west to east, sampled on 6–12 June 2004). Black lines indicate isopycnals of 24.6–26.6 kg m^{-3} steps of 0.1 kg m^{-3} prior to 24.8 kg m^{-3} and 0.2 kg m^{-3} thereafter; and triangles, the position of selected named stations. The red box indicates the isopycnal stretching discussed in the text.

for newly formed NSTM of ~10 m in mid-June [*Jackson et al.*, 2010]. Stations showing a temperature maximum at S < 31 were devoid of any remnant summer halocline. The most stratified region of the water column, chosen as the depth of the Brunt-Väisälä frequency maximum, was rather located below the temperature maximum, at 42.5 (15.9; 51.3) m. This corresponds to the depth of the winter halocline, a remnant of the winter mixed layer that separates Pacific origin waters from the upper-ocean layer. The intrusions observed in June 2004 lied ~15 m beneath a 10.0 (2.8; 21.8) m thick surface mixed layer, which makes of them recent structures that cannot be identified as NSTM. This observation supports the hypothesis of a formation induced by the frontal circulation observed north of Cape Bathurst. These new features will be called surface Temperature Maximum (sTM) to highlight their distinctive origin. Evidence of NSTM in the southeastern Beaufort Sea first appears at the beginning of the summer season. In July 2004 (1 July to 2 August, during the next leg of CASES-2004), near-surface temperature maxima were observed at 17.3 (6.0; 35.7) m, below a summer halocline that coincided with the depth of maximum stratification (located at 2.6 (0.0; 26.6) m depth).

3.1.3.3. Subduction Near Ice Bridge

Only limited data are available to describe the subsurface dynamics in the eastern Amundsen Gulf. The eastern section of transect 100 nevertheless suggests the presence of active processes at the edge of the mesoscale anticyclonic eddy, along the Cape Parry frontal line (Figure 12). Next to the ice bridge, the 24.7 kg m^{-3} isopycnal slopes down as the transect crosses the external side of the eddy revealed by the low-density area in the σ_θ spatial distribution. The sea-surface temperature then increases from −1.4°C at station 108 to 0.0°C at station 111, indicating the presence of warm surface waters advected from the Banks Island area (cf. Figure 7a), before decreasing to −0.3°C at station 112. This station is located east of the cold water mass observable on the SST image of 15 June (labeled AE, Figure 7). At station 111, a minimum of potential temperature is observed at ~40 m where the σ_θ = 24.7–24.8 kg m^{-3} layer appears stretched in the vertical (red box, Figure 12). This minimum exhibits a near-freezing temperature of −1.5°C (freezing point at −1.7°C) and a dissolved oxygen concentration >380 μmol L^{-1} (99.3% oxygen saturation at surface pressure), suggesting an under-ice surface origin; spring microalgae production being typically associated with waters with high O_2 concentration [i.e., *Lansard et al.*, 2012; *Sherr and Sherr*, 2003]. According to profiles collected in the vicinity of the ice bridge (station 108, 15 km west; cf. Figure 1b), near-freezing surface waters bordering the pack ice (θ = −1.6°C) formed a mixed layer $h_{ML} \approx 11$ m thick with σ_θ = 24.7 kg m^{-3}. This temperature minimum follows the σ_θ = 24.7–24.9 kg m^{-3} layer, the thickness of which remained close to $h_i \approx 5$ m along transect 100 (except at the temperature minimum depth, near stations 111–112; Figure 12). Assuming that the fluid parcel observed at the depth of the temperature minimum comes from surface waters flowing on the dense side of the front, near the ice-edge, a frontal subduction driven by frontogenesis could explain the isopycnal stretching observed in CTD data [e.g., *Spall*, 1995]. As $h_{ML} > h_i$, the parcel subducted by the ageostrophic motions active at the Cape Parry frontal line develops an anticyclonic horizontal circulation to compensate for vortex compression and conserves potential vorticity. Similar features were observed in the northern region of the mouth (not shown). In particular, a feature associated with a temperature minimum (θ = −1.6°C) and a negative isentropic vorticity was found to be coherent with the same frontal adjustment process. As a temperature minimum has also been detected at stations 121–123 (cf. Figure 1b), along the western part of transect 100, a northwestward displacement of the eddies generated north of Cape Parry is possible, following the main anticyclonic circulation depicted by the gyre-like structure.

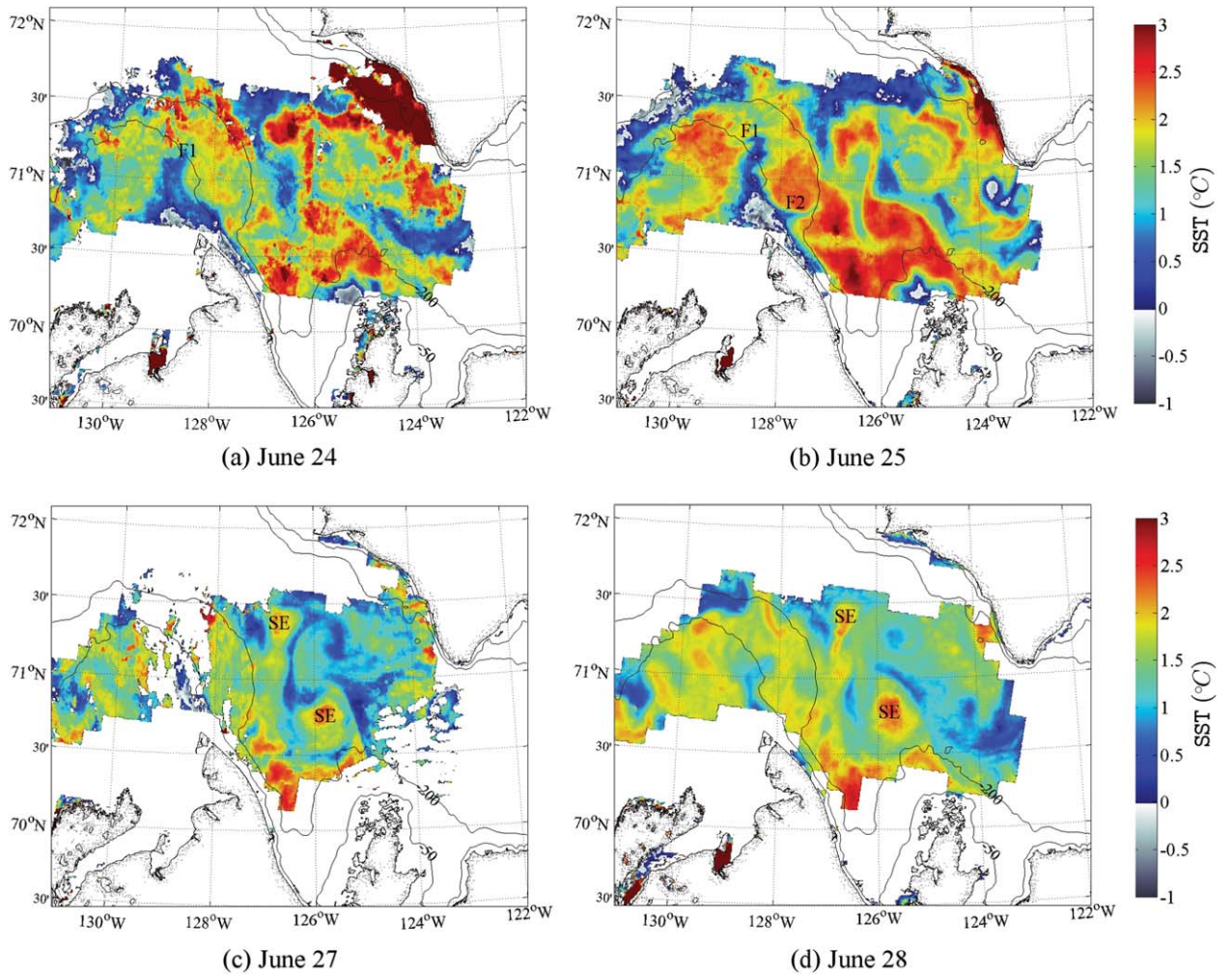

Figure 13. Sea-surface temperature (SST) from the Advanced Very High Resolution Radiometer during the last week of June 2004 (24–28 June). Satellite observations of 24 June are perturbed by an unmasked thin, whitish veil. SE: submesoscale eddies. F: cold filaments.

3.1.4. End of the Frontal Event

After 23 June, the sea-surface temperature underwent major and rapid changes throughout the Amundsen Gulf (Figure 13). The mesoscale eddy progressively disappeared from SST maps, to become hardly distinguishable on 28 June, and areas of high SST cooled noticeably, implying that surface properties were rapidly smoothed out by mixing processes. Some warm submesoscale structures with a horizontal scale of the order of the internal Rossby radius of deformation (∼10 km) are also discernible (labeled SE, Figures 13c and 13d), as were cold upwelling filaments along the 50 m isobath, north of the peninsula (labeled F, Figures 13a and 13b). These offshore-flowing features show evidence of rapid thinning at the wake of the easterly wind event of the end of June (typical speeds of 6.9 m s^{-1} leading to wind stress of 0.07 N m^{-2}; Figure 3), a situation expected when a (submesoscale) filamentary intensification process occurs. Filamentary intensification results from oceanic surface convergence lines that generate a two-celled secondary circulation with strong surface downwelling at its center [*McWilliams et al.*, 2009]. Cold, dense filaments can thus be seen as a double-front experiencing frontogenesis. Time series recorded near the tip of the peninsula, close to the filament observed in SST on 25 June (F2, Figure 13b), show density increase at 30 m depth with simultaneous temperature decrease that suggest entrainment of upwelled waters below the surface (event E3, Figure 4). Opposite changes in density and temperature are observed on 27 June (event E4, Figure 4), which coincides with the reversal of the along-front current at CA06 while moderate, unsteady winds were blowing over the entire region. Warmer, lighter surface waters offshore of the coastal upwelling zone were

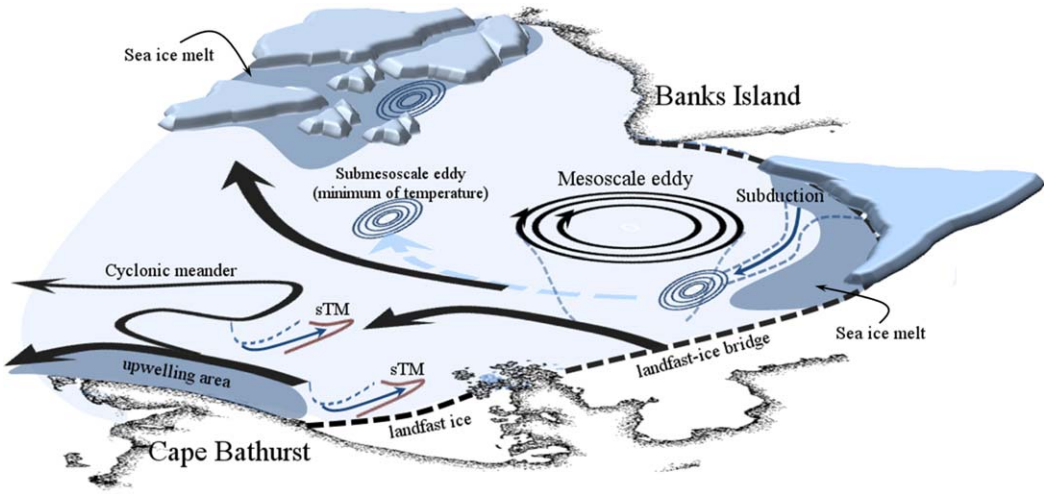

Figure 14. Schematic view of frontal features observed in the southeastern Beaufort Sea during CASES-2004. Blue, dashed lines depict the drawdown of isopycnals at frontal outcrops and in the vicinity of the mesoscale eddy. Thick black arrows indicate the near-surface circulation; thick blue dashed arrow shows the suggested subsurface path followed by the submesoscale eddies generated along the landfast-ice edge (via frontal subduction). Thin blue arrows locate active frontogenetic circulation and red lines show surface intrusions (sTM) generated at the Mackenzie shelf break.

presumably pushed against the Cape and then pulled down over the shelf break (accelerating the restratification of the upper surface). As no intense westerly winds were simultaneously observed, a submesoscale shallow baroclinic instability could be responsible for this observation [*Boccaletti et al*., 2007; *Capet et al*., 2008b] and, consequently, also for the fast frontal collapse that occurred during the last week of June. The front event ends prior to the breakup of the ice bridge.

4. Conclusions

4.1. Fronts in Southeastern Beaufort Sea and Amundsen Gulf in Spring 2004

Coastal upwelling observed north of Cape Bathurst in late spring 2004 followed moderate wind events and can be considered representative of the typical open-sea conditions of the southeastern Beaufort Sea under prevailing easterlies. The volume of cold, dense waters upwelled over Mackenzie Shelf have proven sufficient to influence the near-surface circulation offshore the peninsula and beyond. This process was accompanied by the development of a large, mesoscale anticyclonic eddy in central Amundsen Gulf. Data collected in June 2004 are too sparse to clearly identify the possible mechanism underlying this gyre-like structure, except for a possible response to atmospheric forcing that promote instabilities in the near Banks Island area (cf. mushroom-like currents at the tip of Nelson Head in Figure 13b). SST distribution maps strongly suggest that the frontal lines observed north of Cape Bathurst and Cape Parry were related to the upwelling processes as their formation and evolution are closely linked to each other. Figure 14 summarizes the main frontal features observed in Amundsen Gulf during the spring sampling program of 2004, including the surface intrusions (sTM) generated at the front near the Mackenzie shelf break. The latter are not tied to any summer halocline and cannot be described as near-surface temperature maxima (NSTM), the characteristic anomalies observed at $S < 31$ in the southeastern Beaufort Sea.

A similar pattern of an upwelling zone and a large-scale anticyclone was also observed in satellite data of September–October 2007 [*Sévigny*, 2013]. Intense and persistent easterly winds were blowing over the Amundsen Gulf, giving rise to the major event reported by *Tremblay et al*. [2011]. The frequency of recurrence of these strong density gradient zones is not clear yet, although recent analysis of 11 years of NOAA (AVHRR) images of sea-surface temperature revealed the presence of frequent, but nevertheless year-to-year variable, frontal features in Amundsen Gulf that coincide with the surface fronts described here [*Mustapha*, 2014]. As sea-surface oceanic fronts are ephemeral and highly dependent of external forcing mechanisms for their generation (i.e., upwelling-favorable winds in Amundsen Gulf), the scale used to interpret physical data recorded under ice-free conditions is crucial. Low-pass time series (i.e., seasonal and even

weekly averaging) can smooth-out short upwelling and will lead to results that fail to highlight important processes. It is particularly true near Cape Bathurst where frontal collapse can promote an abrupt reversal of the along-shelf northwestward flow as observed at the end of June–beginning July 2004, southeastward coastal current having been recorded at the tip of the peninsula thereafter. This could explain the divergent conclusions reached by *Ingram et al*. [2008] and *Lanos* [2009] about the general surface circulation inside the Gulf during CASES 2003–2004, described as cyclonic by the former and as anticyclonic by the latter.

4.2. Biological Implications of the Frontal Structures in the Southeastern Beaufort Sea

Advection of nutrient-rich, Pacific deep waters to the surface is the first leading consequence of the wind-driven upwelling front. Doming of the nutricline near Cape Bathurst has likely sustained the phytoplankton bloom observed in the polynya during the first half of June [*Tremblay et al*., 2008; *Gosselin et al*., 2008], enhancing the supply of nitrates to the surface layer on which depends new primary production [*Tremblay et al*., 2011]. However, the possible influences of the large-scale dynamics that occurred in spring 2004 are not restricted to the upwelling area. Along the shelf break, sampling has revealed the quick development of subsurface chlorophyll maxima (SCM), which were in part composed of ice algae [*Tremblay et al*., 2008]. According to these authors, the combination of photoinhibition and substrate-limited nitrate concentrations in the upper layer at (or soon after) ice breakup could have explained the rapid shift of the maximum algal growth rate to a deeper portion of the water column. However, the slantwise frontogenetic circulation active at the northeast corner of the Mackenzie Shelf provides an alternative transport process of the phytoplankton-rich surface waters observed below the surface in the first weeks of June [e.g., *Nagai et al*., 2008]. The surface intrusions generated at the front were precisely observed at a depth of 25 m, which is close to the reported depth of SCM (30–40 m) [*Tremblay et al*., 2008]. Since frontal circulation over the shelf pulls down surface waters initially warmed along the southern edge of the polynya, depths where sTM are observed exhibit slightly higher temperature than in surrounding areas (temperature of -0.4 (-0.7; -0.4)°C instead of -1.2 (-1.3; -1.2)° C, with their 2.5–97.5‰ range). Although no correlation was found between spring and early summer productivity at SCM depth and temperature (while SCM were dominated by diatoms), comparable warming of intermediate waters in late summer-fall could favor phytoplankton growth, low arctic temperatures being then a limiting factor [*Martin et al*., 2012]. Strong westerly (>10 m s^{-1}), upwelling-favorable winds become more frequent from July to September [*Ayles and Snow*, 2002], which increases the possibility of front development and subsequent change in ambient growth conditions of subsurface chlorophyll maxima that persist between 30 and 50 m past late June [*Tremblay et al*., 2008; *Martin et al*., 2013].

The influence of the near-surface frontal circulation on the spatial spreading of biological properties is further revealed by the surface particulate organic carbon (POC) concentration estimated from satellite remote sensing observations [*Forest et al*., 2010]. In June 2004, a thin plume of increased concentration appeared in the prolongation of the peninsula (200 mg C m^{-3}) [see *Forest et al*., 2010, Figure 4], which approximately follows the along-front circulation deduced from CTD data (cf. Figure 8). A slight increase was also noticed at the eastern edge of the mesoscale anticyclonic eddy, near the location of the ice edge ($\approx$100 mg C m^{-3}), suggesting that the physical *and* biological settings of the Amundsen Gulf were influenced by frontal dynamics during open-water period. To date, no specific study has paid attention to the geographical heterogeneity of the ocean biological activity in the southeastern Beaufort Sea and the role played by the underlying large-scale physics. Observations of low phytoplankton biomass and early postbloom conditions [*Gosselin et al*., 2008], and significantly lower sinking export of particulate organic material below the euphotic zone [*Juul-Pedersen et al*., 2010] in central Amundsen Gulf nevertheless suggest that fronts induce specific biological regimes, the mesoscale eddy being one of the most likely determinant features as it may enclose distinct water masses.

In the future, sampling strategy in southeastern Beaufort Sea should take into consideration time and spatial scales of the formation of frontal lines if their objective is to understand the complex physical-biological link that can explain an important component of the peculiar oceanic aspects of the region.

Acknowledgments

We thank correctors for language editing and advices, and are grateful to the scientists and the crews of the CCGS Amundsen for their support in the field. The work was made possible by grants from the ArcticNet Network of Centers of Excellence, the International Polar Year (Circumpolar Flaw Lead Study), and NSERC (Discovery program). This is a Québec-Océan contribution. CTD data used in this research are available through the Polar Data Catalog (https://www.polardata.ca/) and satellite data are made available by Pierre Larouche (DFO, Maurice Lamontagne Institute).

References

Ayles, G., and N. Snow (2002), Canadian Beaufort Sea 2000: The environmental and social setting, *Arctic*, *55*, 4–17.

Barber, D., L. Fortier, and J. Michaud (2008), *On Thin Ice: A Synthesis of the Canadian Arctic Shelf Exchange Study (CASES)*, 215 pp., Aboriginal Issues Press, University of Manitoba, Manitoba.

Barber, D., M. Asplin, Y. Gratton, J. Lukovich, R. Galley, R. Raddatz, and D. Leitch (2010), The International Polar Year (IPY) Circumpolar Flaw Lead (CFL) system study: Overview and the physical system, *Atmos. Ocean*, *48*, 225–243.

Boccaletti, G., R. Ferrari, and B. Fox-Kemper (2007), Mixed layer instabilities and restratification, *J. Phys. Oceanogr.*, *37*, 2228–2250.
Capet, X., J. McWilliams, M. Molemaker, and A. Shchepetkin (2008a), Mesoscale to submesoscale transition in the California Current System. Part I: Flow structure, eddy flux, and observational tests, *J. Phys. Oceanogr.*, *38*, 29–43.
Capet, X., J. McWilliams, M. Molemaker, and A. Shchepetkin (2008b), Mesoscale to submesoscale transition in the California Current System. Part II: Frontal processes, *J. Phys. Oceanogr.*, *38*, 44–64.
Carmack, E., and Y. Kulikov (1998), Wind-forced and internal Kelvin wave generation in Mackenzie Canyon, Beaufort Sea, *J. Geophys. Res.*, *103*, 18,447–18,458.
CIS (2007), Amundsen Gulf animation 1980–2007. [Available at http:\\ice-glaces.ec.gc.ca\content_contenu\anim\amundsen_animation.gif.]
D'Asaro, E., C. Lee, L. Rainville, R. Harcourt, and L. Thomas (2011), Enhanced turbulence and energy dissipation at ocean fronts, *Science*, *332*, 318–322.
Forest, A., M. Sampei, R. Makabe, H. Sasaki, D. Barber, Y. Gratton, P. Wassmann, and L. Fortier (2008), The annual cycle of particulate organic carbon export in Franklin Bay (Canadian Arctic): Environmental control and food web implications, *J. Geophys. Res.*, *113*, C03S05, doi: 10.1029/2007JC004262.
Forest, A., S. Bélanger, M. Sampei, H. Sasaki, C. Lalande, and L. Fortier (2010), Three-year assessment of particulate organic carbon fluxes in Amundsen Gulf (Beaufort Sea): Satellite observations and sediment trap measurements, *Deep Sea Res., Part I*, *57*, 125–142.
Galbraith, P., and P. Larouche (2011), Sea-surface temperature in Hudson Bay and Hudson Strait in relation to air temperature and ice cover breakup, 1985–2009, *J. Mar. Syst.*, *87*, 66–78.
Gosselin, M., et al. (2008), Light, nutrients and primary production, in *On Thin Ice: A Synthesis of the Canadian Arctic Shelf Exchange Study (CASES)*, edited by L. Fortier, D. G. Barber, and J. Michaud, pp. 13–38, Aboriginal Issues Press, Winnipeg, Canada.
Haynes, P., and J. Anglade (1997), The vertical-scale cascade in atmospheric tracers due to large-scale differential advection, *J. Atmos. Sci.*, *54*, 1121–1136.
Hoskins, B., and F. Bretherton (1972), Atmospheric frontogenesis models: Mathematical formulation and solution, *J. Atmos. Sci.*, *29*, 11–37.
Ingram, R., W. Williams, B. Van Hardenberg, J. Dawe, and E. Carmack (2008), Seasonal circulation over the Canadian Beaufort Shelf, in *On Thin Ice: A Synthesis of the Canadian Arctic Shelf Exchange Study (CASES)*, edited by L. Fortier, D. G. Barber, and J. Michaud, pp. 13–38, Aboriginal Issues Press, Winnipeg, Canada.
Jackson, J., E. Carmack, F. McLaughlin, S. E. Allen, and R. Ingram (2010), Identification, characterization, and change of the near-surface temperature maximum in the Canada Basin, 1993–2008, *J. Geophys. Res.*, *115*, C05021, doi:10.1029/2009JC005265.
Johnston, T., O. Cheriton, J. Pennington, and F. Chavez (2009), Thin phytoplankton layer formation at eddies, filaments, and fronts in a coastal upwelling zone, *Deep Sea Res.*, Part II, *56*, 246–259.
Johnston, T., D. L. Rudnick, and E. Pallàs-Sanz (2011), Elevated mixing at a front, *J. Geophys. Res.*, *116*, C11033, doi:10.1029/2011JC007192.
Juul-Pedersen, T., C. Michel, and M. Gosselin (2010), Sinking export of particulate organic material from the euphotic zone in the eastern Beaufort Sea, *Mar. Ecol. Prog. Ser.*, *410*, 55–70.
Klein, P., A. M. Treguier, and B. Hua (1998), Three-dimensional stirring of thermohaline fronts, *J. Mar. Res.*, *56*, 589–612.
Klein, P., B. L. Hua, G. Lapeyre, X. Capet, S. Le Gentil, and H. Sasaki (2008), Upper ocean turbulence from high-resolution 3D simulations, *J. Phys. Oceanogr.*, *38*, 1748–1763.
Lanos, R. (2009), Circulation régionale, masses d'eau, cycles d'évolution et transports entre la mer de Beaufort et de golfe d'Amundsen, PhD thesis, 245 pp., INRS-Centre Eau, Terre et Environnement, Québec, Canada.
Lansard, B., A. Mucci, L. Miller, R. Macdonald, and Y. Gratton (2012), Seasonal variability of water mass distribution in the southeastern Beaufort Sea determined by total alkalinity and δ18O, *J. Geophys. Res.*, *117*, C03003, doi:10.1029/2011JC007299.
Mahadevan, A., and A. Tandon (2006), An analysis of mechanisms for submesoscale vertical motion at ocean fronts, *Ocean Modell.*, *14*, 241–256.
Martin, J., J. Tremblay, and N. Price (2012), Nutritive and photosynthetic ecology of subsurface chlorophyll maxima in Canadian Arctic waters, *Biogeosciences*, *9*, 5353–5371.
Martin, J., D. Dumont, and J. É. Tremblay (2013), Contribution of subsurface chlorophyll maxima to primary production in the coastal Beaufort Sea (Canadian Arctic): A model assessment, *J. Geophys. Res. Oceans*, *118*, 5873–5886, doi:10.1002/2013JC008843.
May, B., and D. Kelley (2001), Growth and steady state stages of thermohaline intrusions in the Arctic Ocean, *J. Geophys. Res.*, *106*, 16,783–16,794.
McLaughlin, F., E. Carmack, R. Macdonald, and J. Bishop (1996), Physical and geochemical properties across the Atlantic/Pacific water masses front in the southern Canadian Basin, *J. Geophys. Res.*, *101*, 1183–1197.
McLaughlin, F., E. Carmack, R. Macdonald, H. Melling, J. Swift, P. Wheeler, B. Sherr, and E. Sherr (2004), The joint roles of Pacific and Atlantic-origin waters in the Canada Basin, 1997–1998, *Deep Sea Res., Part I*, *51*, 107–128.
McPhee, M., A. Proshutinsky, J. H. Morison, M. Steele, and M. Alkire (2009), Rapid change in freshwater content of the Arctic Ocean, *Geophys. Res. Lett.*, *36*, L10602, doi:10.1029/2009GL037525.
McWilliams, J., M. Molemaker, and E. Olafsdottir (2009), Linear fluctuation growth during frontogenesis, *J. Phys. Oceanogr.*, *39*, 3111–3129.
Molemaker, M., J. McWilliams, and X. Capet (2010), Balanced and unbalanced routes to dissipation in an equilibrated Eady flow, *J. Fluid Mech.*, *654*, 35–63.
Mustapha, S. (2014), Étude de la variabilité spatio-temporelle des processus physiques et biologiques dans la mer de Beaufort par télédétection et dans un contexte de changements climatiques dans l'océan Arctique, PhD thesis, 238 pp., Université de Sherbrooke, Sherbrooke, Canada.
Nagai, T., A. Tandon, N. Gruber, and J. McWilliams (2008), Biological and physical impacts of ageostrophic frontal circulations driven by confluent flow and vertical mixing, *Dyn. Atmos. Oceans*, *45*, 229–251.
Nagai, T., A. Tandon, H. Yamazaki, M. Doubell, and S. Gallager (2012), Direct observations of microscale turbulence and thermohaline structure in the Kuroshio front, *J. Geophys. Res.*, *117*, C08013, doi:10.1029/2011JC007228.
Perovich, D., J. Richter-Menge, K. Jones, and B. Light (2008), Sunlight, water, and ice: Extreme Arctic sea ice melt during the summer of 2007, *Geophys. Res. Lett.*, *35*, L11501, doi:10.1029/2008GL034007.
Pollard, R., and L. Regier (1992), Vorticity and vertical circulation at an ocean front, *J. Phys. Oceanogr.*, *22*, 609–625.
Sévigny, C. (2013), Mélange et fronts océaniques dans les couches supérieures du golfe d'Amundsen et de l'Arctique canadien, PhD thesis, 276 pp., INRS-Centre Eau, Terre et Environnement, Québec, Canada.
Sherr, B., and E. Sherr (2003), Community respiration/production and bacterial activity in the upper water column of the central Arctic Ocean, *Deep Sea Res., Part I*, *50*, 529–542.
Smith, K., and R. Ferrari (2009), The production and dissipation of compensated thermohaline variance by mesoscale stirring, *J. Phys. Oceanogr.*, *39*, 2477–2501.
Spall, M. (1995), Frontogenesis, subduction, and cross-front exchange at upper ocean fronts, *J. Geophys. Res.*, *100*, 2543–2557.

Stroeve, J., M. Serreze, S. Drobot, S. Gearheard, M. Holland, J. Maslanik, W. Meier, and T. Scambos (2008), Arctic sea ice extent plummets in 2007, *Eos Trans. AGU*, *89*(2), 13–14.

Thomas, L., J. Taylor, R. Ferrari, and T. Joyce (2013), Symmetric instability in the gulf stream, *Deep Sea Res.*, Part II, *91*, 96–110.

Tremblay, J. É., and J. Gagnon (2009), The effects of irradiance and nutrient supply on the productivity of Arctic waters: A perspective on climate change, in *Influence of climate change in the changing Arctic and sub-Arctic conditions. NATO Science for Peace and Security Series – C: Environmental security*, edited by J. C. J. Nihoul and A. G. Kostianoy, pp. 73–93, Springer, Dordrecht, Netherlands.

Tremblay, J. É., K. Simpson, J. Martin, L. Miller, Y. Gratton, D. Barber, and N. M. Price (2008), Vertical stability and the annual dynamics of nutrients and chlorophyll fluorescence in the coastal, southeast Beaufort Sea, *J. Geophys. Res.*, *113*, C07S90, doi:10.1029/2007JC004547.

Tremblay, J. É., et al. (2011), Climate forcing multiplies biological productivity in the coastal Arctic Ocean, *Geophys. Res. Lett.*, *38*, L18604, doi:10.1029/2011GL048825.

UNESCO-IOC (2010), *GTSPP Real-Time Quality Control Manual*, First Revised Edition. (IOC Manuals and Guides No. 22, Revised Edition.) United Nations Educational, Scientific and Cultural Organization, Paris.

Williams, W., and E. Carmack (2008), Combined effect of wind-forcing and isobath divergence on upwelling at Cape Bathurst, Beaufort Sea, *J. Mar. Res.*, *66*, 645–663.

Zakardjian, B., and L. Prieur (1998), Biological and chemical signs of upward motions in permanent geostrophic fronts of the Western Mediterranean, *J. Geophys. Res.*, *103*, 27,849–27,866.